Supplementary material of: "An Efficient Approach for Controlling the Crystallization, Strain, and Defects of the Perovskite Film in Hybrid Perovskite Solar Cells Through Antisolvent Engineering"
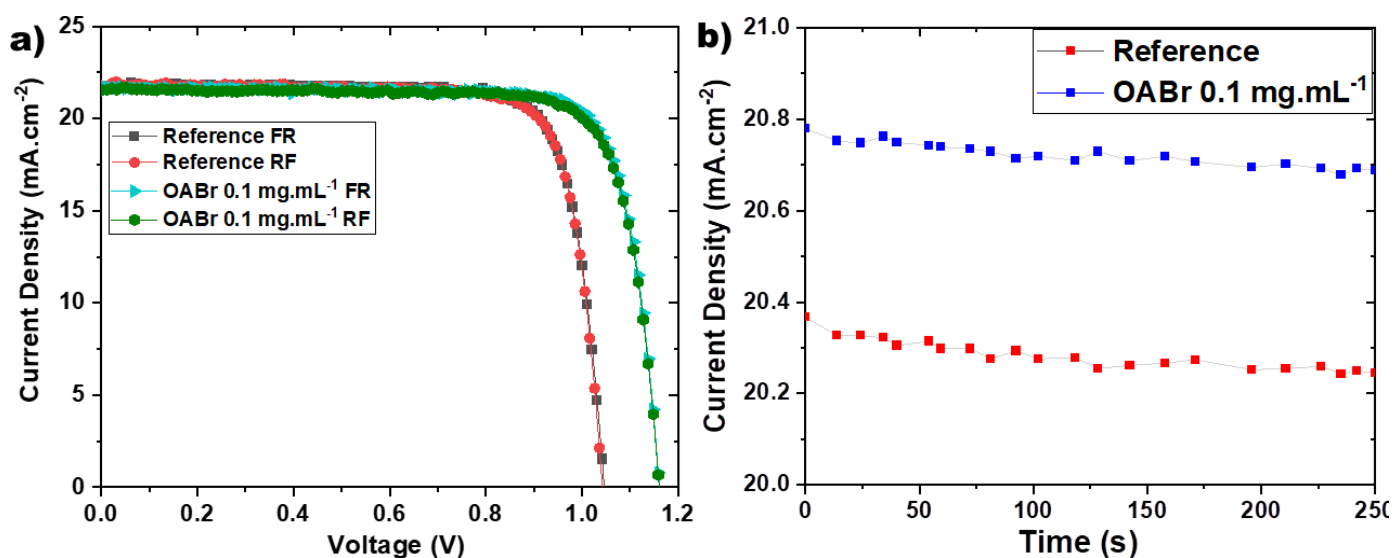

Figure S1. a) Forward and reverse J-V scans of the reference and optimal OABr treated device with OABr concentration of 0.1 mgmL^{-1}. **b)** Stabilized current density at fixed voltage of 0.9 V for reference and 0.95 V for OABr 0.1 mgmL^{-1} devices.
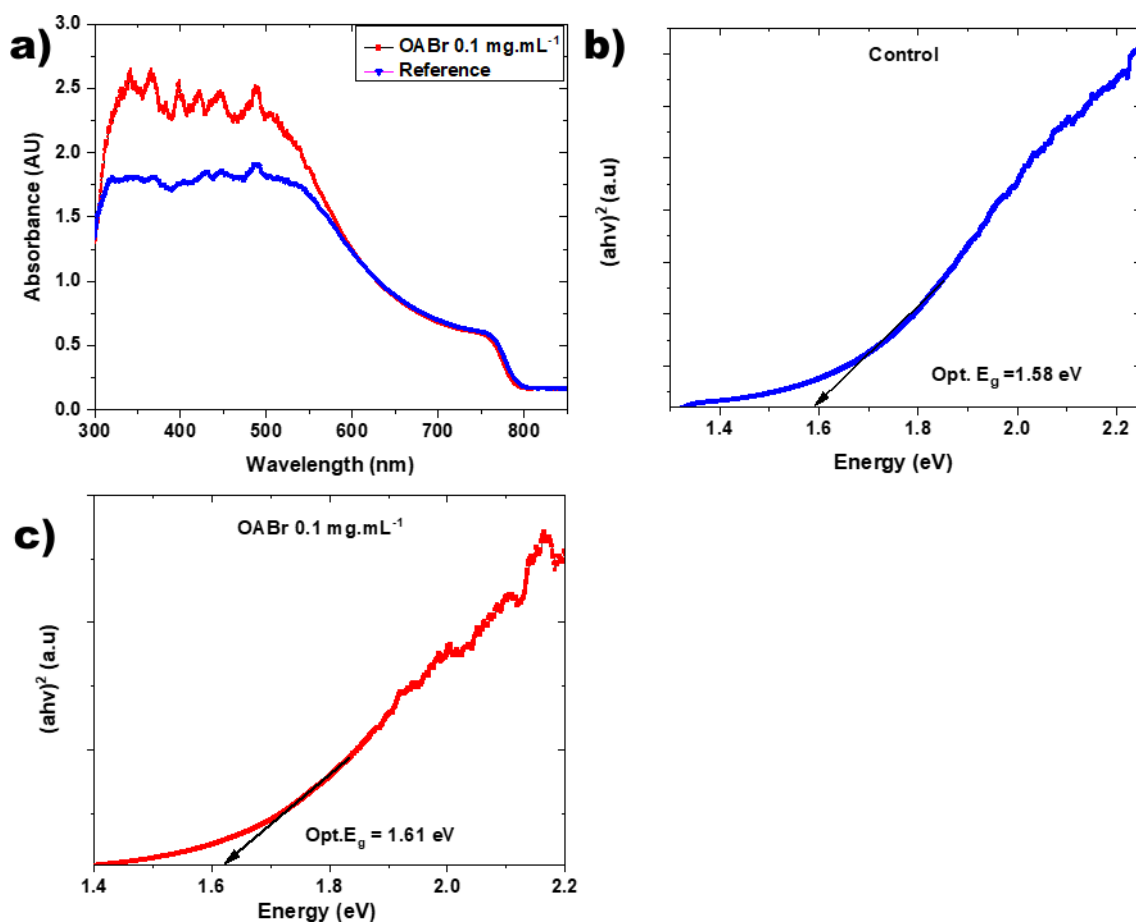

Figure S2. a) Uv-Vis absorption spectra of reference and OABr 0.1 mgmL^{-1} perovskites, and the respective Tauc plots for **b)** the reference and **c)** the OABr 0.1 mgmL^{-1} samples, respectively. The optical band gaps were estimated from extrapolating the linear part to the energy axis.
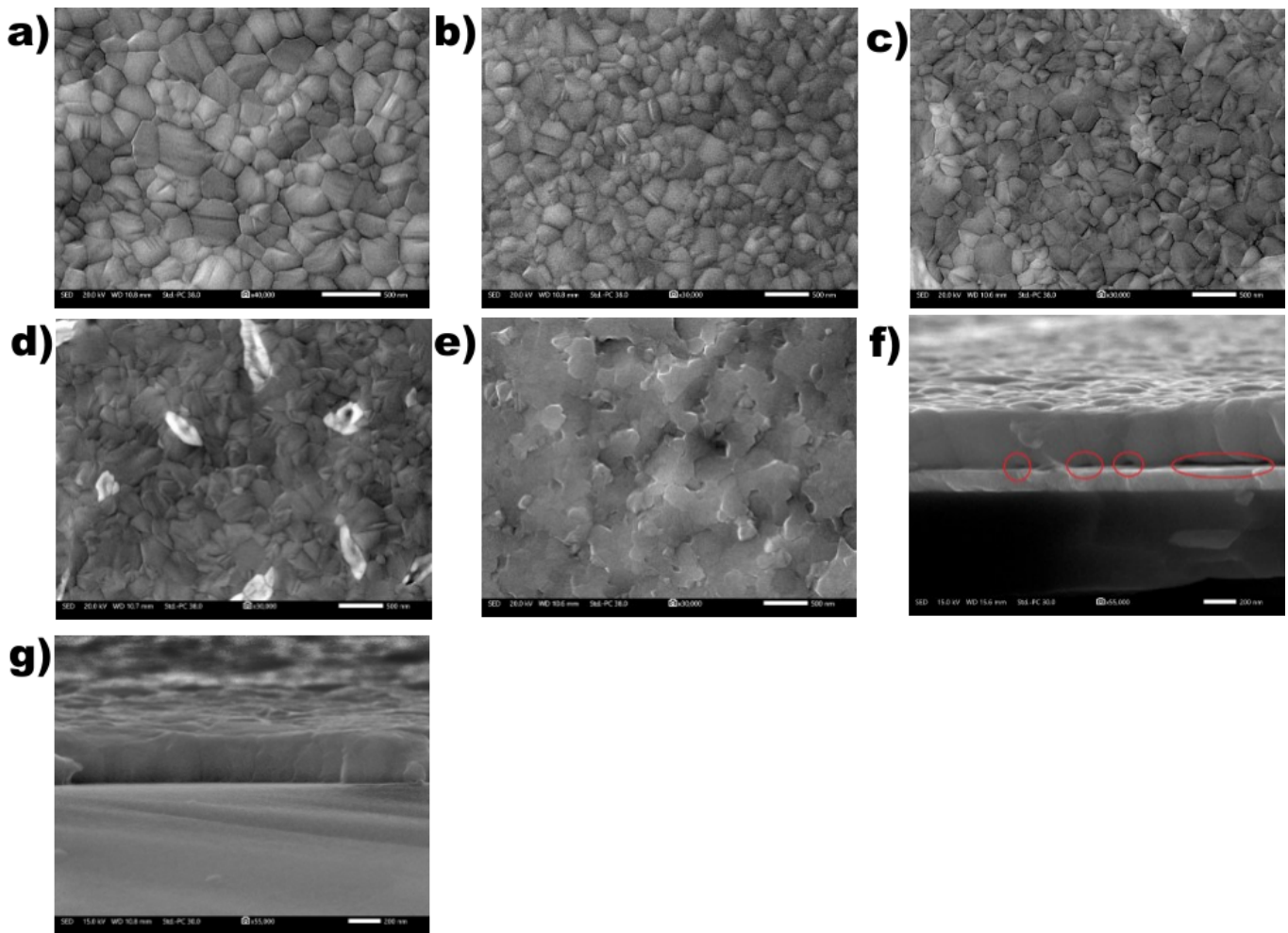
Figure S3. Top-view SEM images of a) reference, and OABr treated samples with OABr concentrations of b) 0.01 mgmL^{-1}, c) 0.05 mgmL^{-1}, d) 0.1 mgmL^{-1}, and e) 0.25 mgmL^{-1}. Side-view SEM images of f) reference, and g) 0.1 mgmL^{-1} OABr treated perovskite. The red oval curves in panel f) mark the pin-holes at the PTAA/Perovskite interface.

Table S1. The mean grain size as estimated ftom the top-view SEM images.

Sample	Mean grain size [nm]
Reference	180±14
0.01 mgmL^{-1}	182±19
0.05 mgmL^{-1}	184±20
0.1 mgmL^{-1}	244±23
0.25 mgmL-1	487±25

Figure S4. AFM topography images of the perovskite surface a) without treatment, and treated with OABr at concentrations of b), 0.01 mgmL^{-1}, c) 0.05 mgmL^{-1} and d) 0.1 mgmL^{-1}. The AFM images were processed to better visualize the perovskite grains.

Table S2. Mean grain size and RMS roughness as estimated from AFM topography images.

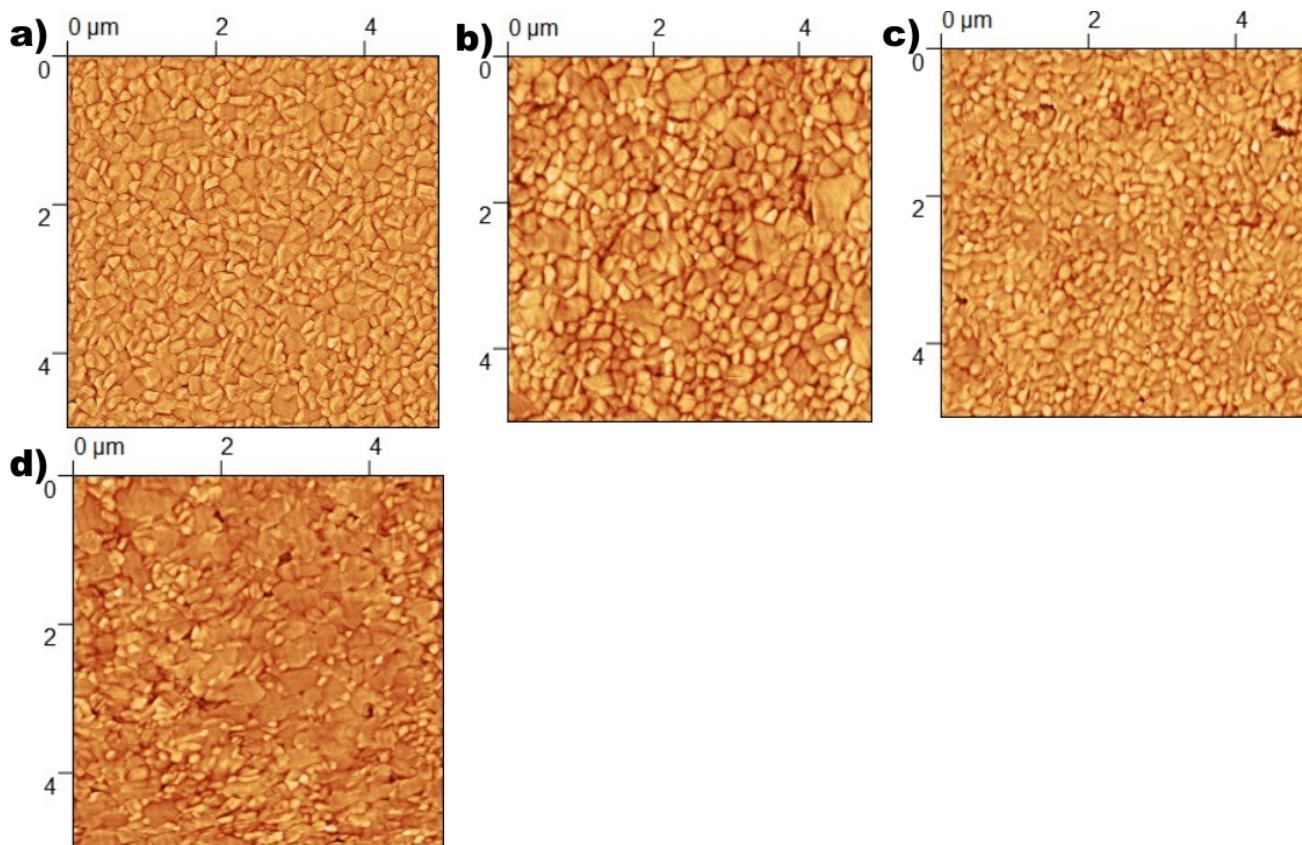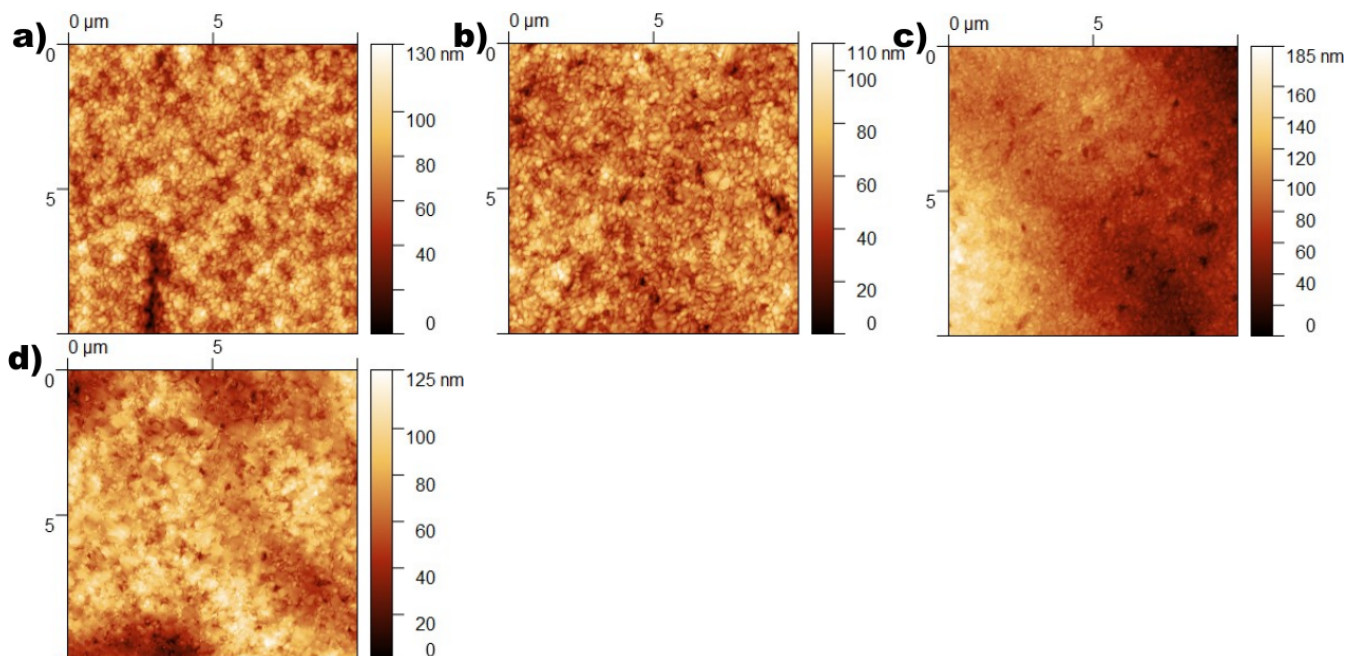| Sample	Mean grain size [nm]	RMS [nm]
Reference	160±12	15.33
0.01 mgmL^{-1}	204±18	12.49
0.05 mgmL^{-1}	203±8	29.03
0.1 mgmL^{-1}	270±10	16.91

Figure S5. Raw AFM topography images of the perovskite surface a) without treatment, and treated with OABr at concentrations of b), 0.01 mgmL^{-1}, c) 0.05 mgmL^{-1} and d) 0.1 mgmL^{-1}.
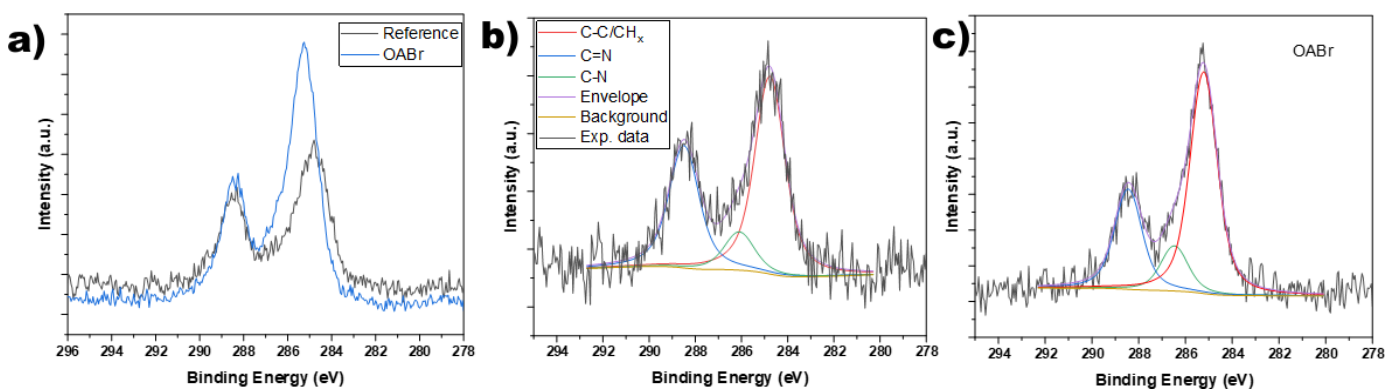

Figure S6. XPS C1s core peaks of the reference perovskite and treated with 0.1 mgmL^{-1} OABr. Panel a) shows the C1s core peaks of both samples. The deconvolution of C1s core peaks is shown in panel b) for the reference and in panel c) for the OABr 0.1 mgmL^{-1} samples, respectively.
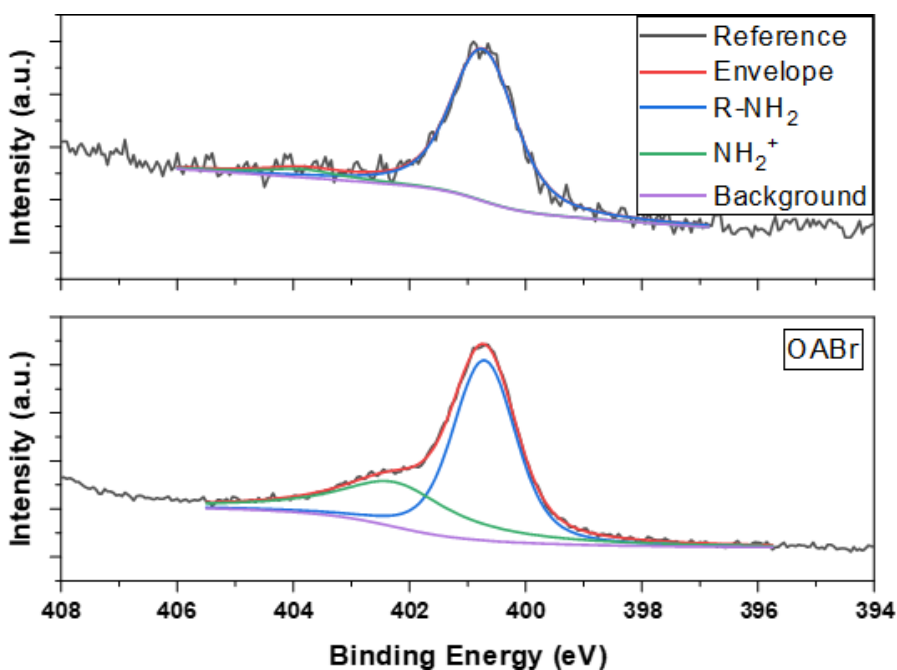
Figure S7. The deconvolution of XPS N1s core peaks of a) reference and b) OABr 0.1 mgmL^{-1} treated perovskites.
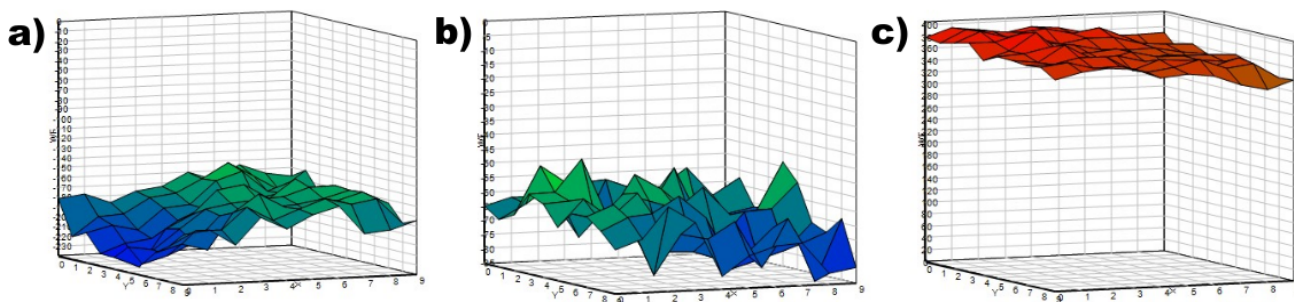
Figure S8. Scanning Kelvin probe 2D mapping images depicting the distribution of CPD on the surface of a) reference, b) 0.05 mgmL^{-1}, and c) 0. 1 mgmL^{-1} of OABr treated perovskites.

Figure S9. Contact angle measurements of a droplet of PC$_{61}$BM iinn CB on perovskite surface a) reference, and treated with OABr at concentrations of b) 0.01 mgmL^{-1}, c) 0.05 mgmL^{-1}, d) 0.1 mgmL^{-1} and e) OABr 0.25 mgmL^{-1}

Figure S10. APS measurements of the a) reference perovskite and b) perovskite treated with 0.1 mgmL^{-1} OABr. In panel c) are plotted the XPS spectra of the VB region.
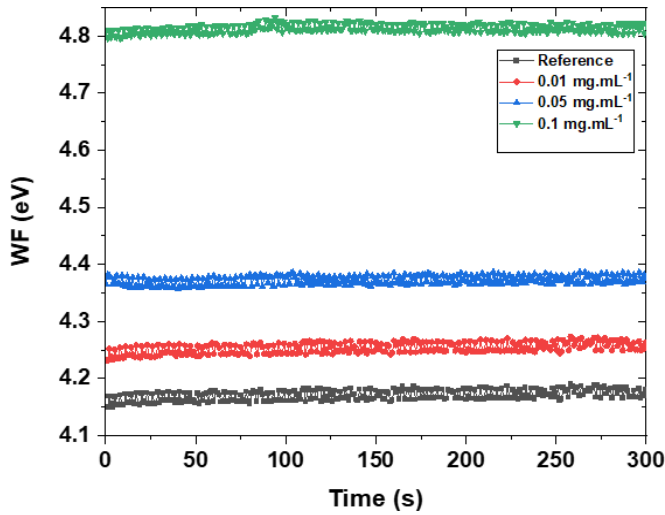
Figure S11. WF measurements in the dark of the perovskite a) without treatment and treated with OABr at concentrations of 0.01, 0.05, and 0.1 mgmL⁻¹.
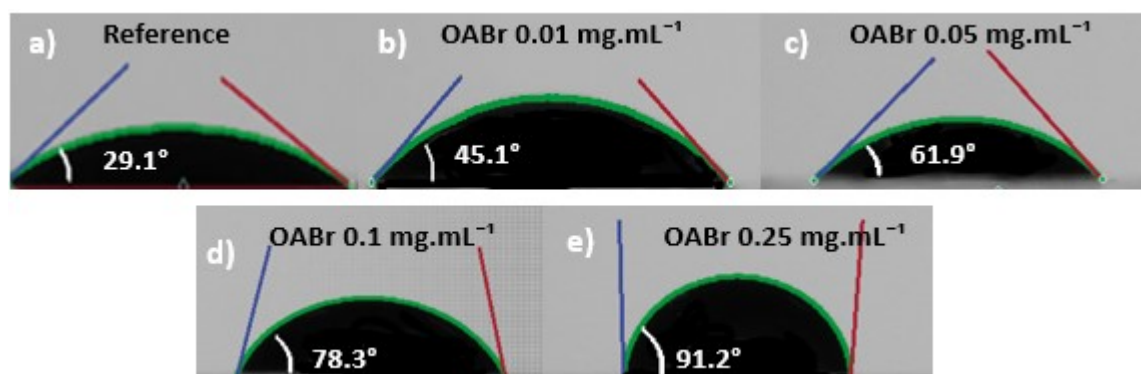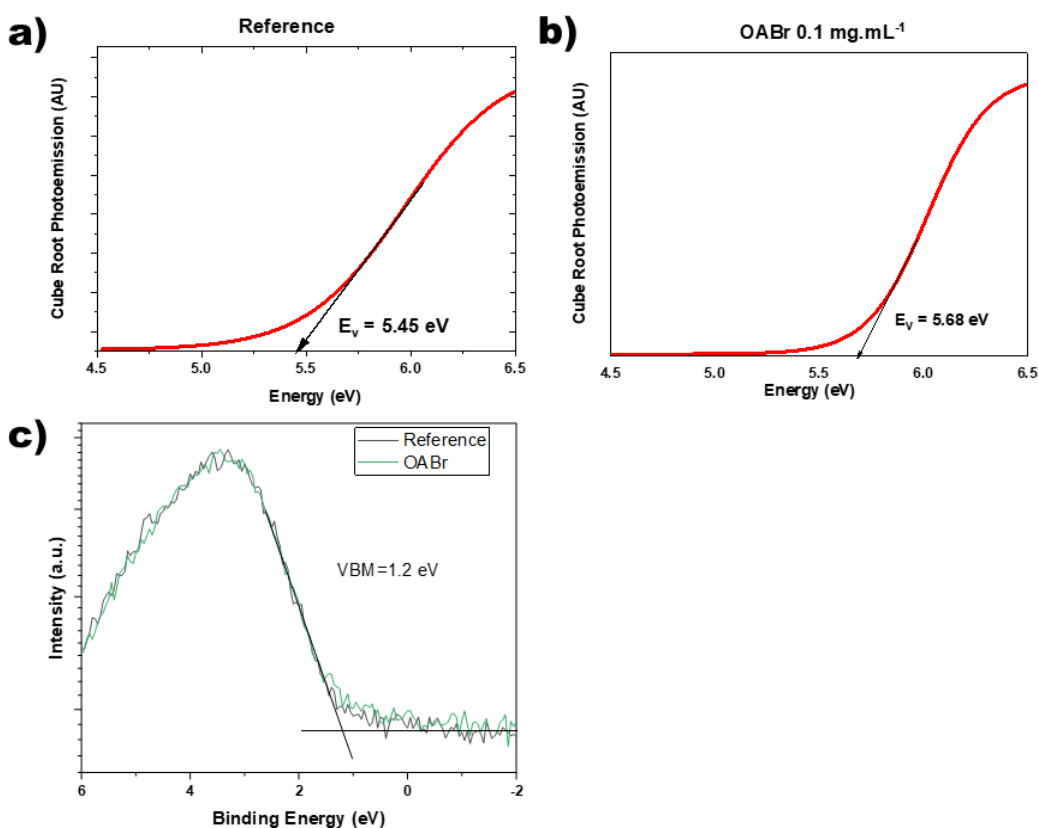
Table S3. Stabilized WF values estimated form the dark Kelvin probe measurements.

OABr concentration [mgmL⁻¹]	WF [eV]
Reference	-4.18
0.01	-4.25
0.05	-4.39
0.1	-4.8
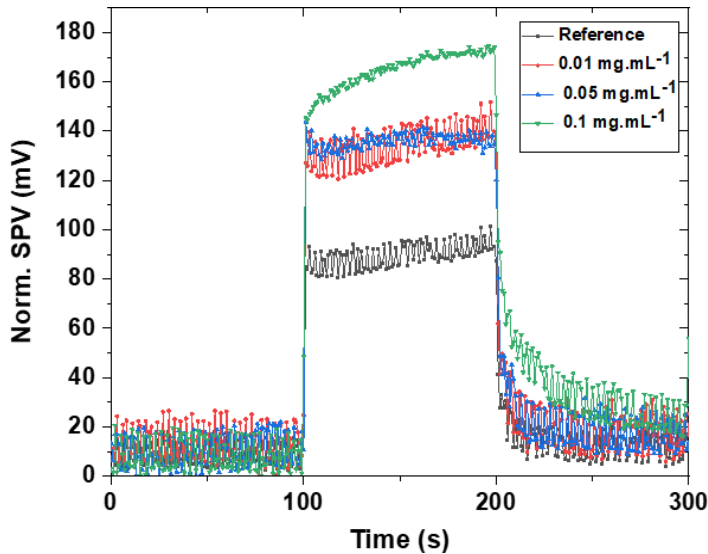
Figure S12. SPV measurements of the perovskite and of OABr treated samples. The SPV curves were normalized to lowest value.

Fitting of the SPV decay

The SPV decay after the light was turn off, which is shown in Figure S12 after 200 s, was fitted to the exponential decay function:

$$y = y_0 + A * exp(-tx) \quad (S1)$$

The values of the decay rate constant t are listed in table S4.

Table S4. The values of the decay rate parameter extracted from the decay SPV data of Figure S12.

OABr concentration [mgmL⁻¹]	t [s⁻¹]
Reference	0.365
0.01	0.271

0.05	0.240
0.1	0.129

Table S4 Ratios of the photovoltaic parameters calculated according to SQ limit for ideal solar cells with band gaps of 1.59 and 1.61 eV. The values in the brackets correspond to ratios calculated from the experimental measurements in Table 1 for the reference (E$_g$=1.59 eV) and for the OABr 0.1 mgmL^{-1} sample (E$_g$=1.61 eV).

$J_{sc}^{SQ,1.59}/J_{sc}^{SQ,1.61}$	$V_{oc}^{SQ,1.59}/V_{oc}^{SQ,1.61}$	$FF^{SQ,1.59}/FF^{SQ,1.61}$	$PCE^{SQ,1.59}/PCE^{SQ,1.61}$
1.028 (1.007)	0.986 (0.882)	0.999 (0.986)	1.013 (0.875)

V$_{oc}$ loss analysis

The total V$_{oc}$ loss, ΔV, can be described by the equation listed below:

$$q\Delta V = E_g - qV_{oc} = \left(E_g - qV_{oc}^{SQ}\right) + \left(qV_{oc}^{SQ} - qV_{oc}^{rad}\right) + \left(qV_{oc}^{rad} - qV_{oc}\right) = \Delta E_1 - \Delta E_2 - \Delta E_3 \quad (1)$$

Where q is the elementary charge, ΔV is total voltage loss, E$_g$ is the band gap of the perovskite, V$_{oc}^{SQ}$ is maximum theoretic V$_{oc}$ under the Shockley-Queisser limit, V$_{oc}^{rad}$ is the V$_{oc}$ when only radiative recombination is present.

The third loss, ΔE_3 express the losses due to non-radiative recombination and it can be calculated following the method of L. Krückemeier et.al [1]. Assuming an Urbach energy of 16 meV and using the EQE spectra of the best reference and OABr enabled devices, we estimate ΔE_3 and V$_{oc}^{rad}$ as shown in table S4. The values of V$_{oc}^{SQ}$ were acquired from tubulated values [2]. Next, we calculate the ΔE_2 losses related to radiative recombination from a non-ideal absorption spectrum, for example due to a non-abrupt absorption onset and the presence of sub-gap states. The ΔE_1 losses are ascribed to radiative recombination from a semiconductor where the absorption spectrum is simplified to a step function. The total V$_{oc}$ losses, ΔV are calculated according to equation 1.

Table S5. The V$_{oc}^{rad}$ and V$_{oc}^{SQ}$ and values as estimated according to references [1] and [2], respectively. The total V$_{oc}$ loss wass calculated according to equation 1.

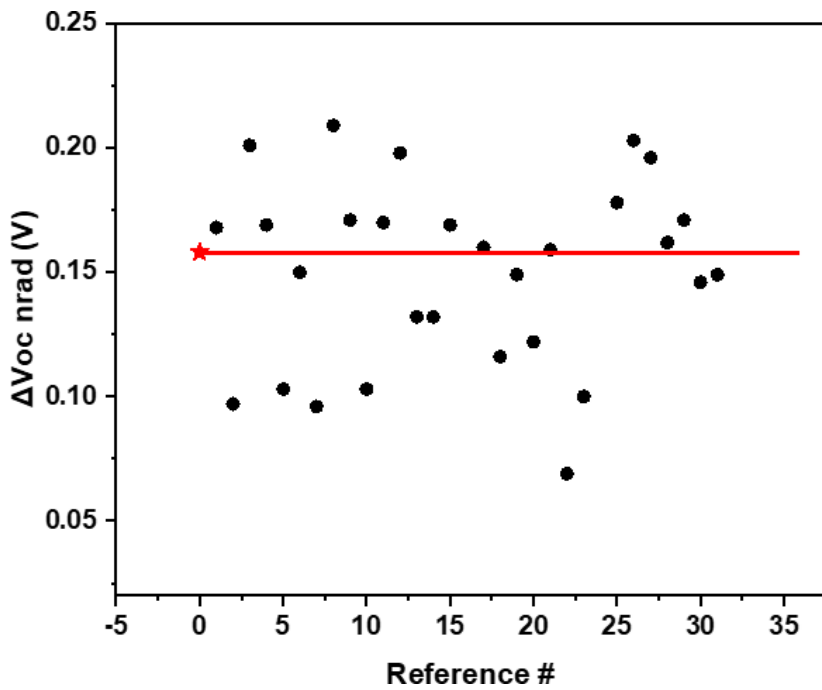| Sample	V$_{oc}$ (V)	V$_{oc}^{SQ}$ (V)	V$_{oc}^{rad}$ (V)	ΔE_1 (mV)	ΔE_2 (mV)	ΔE_3 (mV)	ΔV (mV)
Reference	1.023	1.317	1.3052	273	12	282	567
OABr 0.1 mgmL-1	1.160	1.336	1.3195	274	17	159	450

Figure S13. Literature comparison of non-radiative losses of devices in our work (star point) with inverted perovskite devices with similar structure.
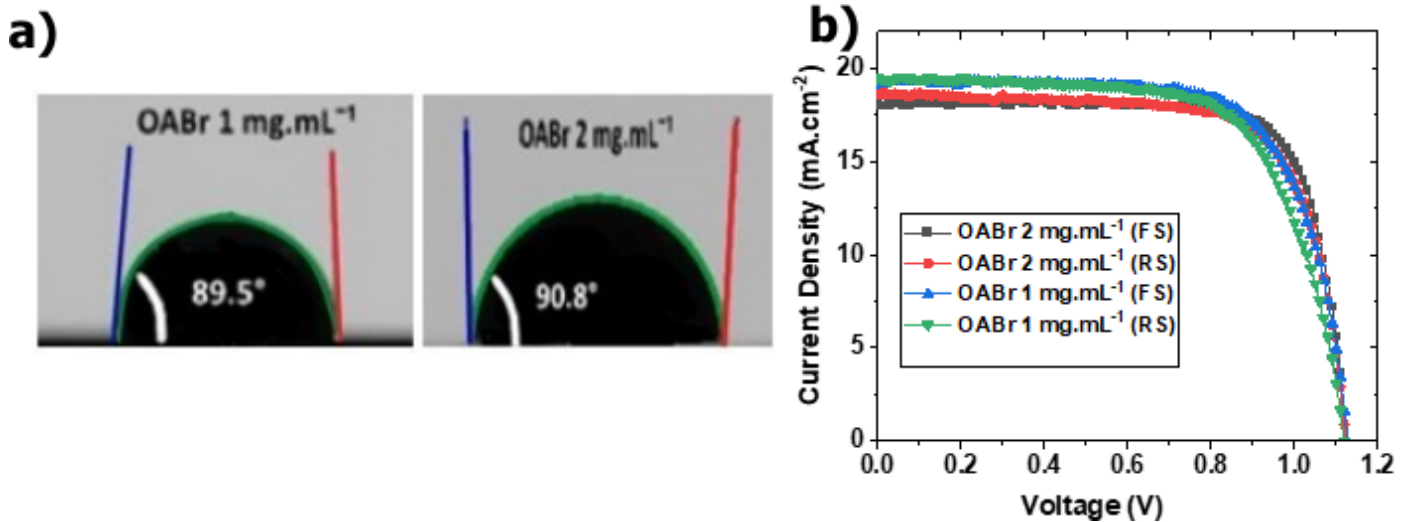
Figure S14. a) Contact angle images of a $PC_{61}BM$ in CB droplet on the surface of perovskite treated by spin coating an OABr layer from solutions of 1 and 2 $mgmL^{-1}$, b) J-V plots of devices, which implement OABr deposited on the perovskite via spin coating from OABr solutions of in 1 and 2 $mgmL^{-1}$ CB.

Table S6. Literature review of inverted devices with similar structure with our devices. The nonradiative losses ΔV_{oc}^{nrad} were calculated based on the band gap and the SQ limit.

Device Architecture	Voc	Eg	ΔV_{oc}^{nrad}	Reference
	[V]	[eV]	[V]	#
ITO/PTAA/PVSK:OABr/PCBM/BCP/Ag	1.160	1.61	0.159	This work
ITO/NiO$_x$/PVSK:PPP/PCBM:C60/BCP/Cr/Au	1.131	1.59	0.168	[3]
ITO/PTAA/F-PEAI/PVSK/PEAI/PCBM/BCP/Ag	1.184	1.57	0.097	[4]
ITO/MeO-2PACkz/PVSK/PCBM:GF/	1.098	1.59	0.201	[5]

ITO/PTAA/PVSK:KBF4/PCBM/BCP/Ag	1.130	1.59	0.169	[6]
ITO/PTAA/PVSK:BDAI$_2$/PCBM/BCP/Ag	1.15	1.54	0.103	[7]
ITO/NiO$_x$/Al$_2$O$_3$/PVSK/PCBM/Ag	1.14	1.58	0.15	[8]
ITO/NiO$_x$/MS-OC/PVSK/PCBM/BCP/Au	1.128	1.51	0.096	[9]
ITO/NiO$_x$/PVSK/PHMT/PCBM/BCP/Cr/Au	1.10	1.60	0.209	[10]
ITO/PTAA/PVSK/TOAB/PCBM/BCP/Ag	1.11	1.56	0.171	[11]
ITO/PTAA:F4-TCNQ/PMMA/PVSK/PCBM/Bphen/Al	1.168	1.56	0.103	[12]
ITO/NiO NPs/PVSK:HEA/PCBM/ZnO NPs/Ag	1.12	1.58	0.17	[13]
FTO/Cs:NiO$_x$/PVSK/PCBM/ZrAcac/Ag	1.120	1.61	0.198	[14]
ITO/TPE-S/PVSK/PCBM/ZnO/Ag	1.13	1.55	0.132	[15]
ITO/PTAA/PFN-Br:PEAI/PVSK/PCBM/BCP/Cu	1.130	1.55	0.132	[16]
ITO/PTAA:MoO$_3$/PVSK/PCBM/BCP/Au	1.14	1.60	0.169	[17]
ITO/NiO$_x$/PTAA/CsFA/F/BCP/Ag	1.06	1.60	1.249	[18]
ITO/NiO$_x$/PVSK/PCBM:C60/BCP/Cr/Au	1.139	1.59	0.16	[19]
ITO/PTAA/PVSK/BHJ/Zr(acac)$_4$/Ag	1.146	1.55	0.116	[20]
ITO/CzPFO :PTAA/PVSK/PCBM/C60/LiF/Cu	1.16	1.6	0.149	[21]
ITO/PTAA/PVSK/PCBM/BCP/Ag	1.14	1.55	0.122	[22]
ITO/PTAA/PVSK/PCBM/BCP/Cu	1.15	1.6	0.159	[23]
ITO/NiO$_x$/PTAA/2DPSVK/PCBM/BCP/Ag	1.24	1.6	0.069	[24]
ITO/NiO$_x$/PTAA/PVSK/PCBM/BCP/Ag	1.19	1.58	0.1	[25]
ITO/PTAA/PSVK/ZnO/C60	1.14	1.91	0.459	[26]
ITO/PTAA:doped/PVSK/PCBM/Ag	1.14	1.61	0.178	[27]
ITO/PTAA/PFN/2DPSVK/PCBM/BCP/Ag	1.19	1.69	0.203	[28]
ITO/NiO/2PACz/PVSK/PCBM/BCP/Cu	1.16	1.65	0.196	[29]
FTO/NiOx/PSVK/C60:Co-TiO2/BCP/Ag	1.10	1.55	0.162	[30]
ITO/HTL/PSVK/PCBM/Bphen/Ag	1.091	1.55	0.171	[31]
ITO/poly-TPD/2PACz/PVSK/2-TEAI/PCBM/BCP/Ag	1.20	1.64	0.146	[32]
ITO/NiOx:TTS/PVSK/PCBM:C60/BCP/Au	1.15	1.59	0.149	[33]

Table S7. The extracted photovoltaic parameters from the JV curves of Figure S14.

Sample	PCE [%]	FF [%]	V_{oc} [V]	J_{sc} [mAcm^{-2}]
OABr 1 mgmL^{-1} FS	16.17	74.69	1.127	19.21
OABr 1 mgmL^{-1} RS	15.58	71.55	1.118	19.48
OABr 2 mgmL^{-1} FS	16.55	77.51	1.125	18.99
OABr 2 mgmL^{-1} RS	15.95	75.05	1.123	18.93

References

[1]   L. Krückemeier, U. Rau, M. Stolterfoht, T. Kirchartz, *Adv. Energy Mater.* **2020**, *10*, 1902573.

[2]   S. Rühle, *Sol. Energy* **2016**, *130*, 139.

[3]   Q. Cao, Y. Li, H. Zhang, J. Yang, J. Han, T. Xu, S. Wang, Z. Wang, B. Gao, J. Zhao, X. Li, X. Ma, S. M. Zakeeruddin, W. E. I. Sha, X. Li, M. Grätzel, *Sci. Adv.* **2021**, *7*, eabg0633.

[4]   M. Degani, Q. An, M. Albaladejo-Siguan, Y. J. Hofstetter, C. Cho, F. Paulus, G. Grancini, Y. Vaynzof, *Sci. Adv.* **2021**, *7*, eabj7930.

[5]   A. Zanetta, I. Bulfaro, F. Faini, M. Manzi, G. Pica, M. De Bastiani, S. Bellani, M. I. Zappia, G. Bianca, L. Gabatel, J. Panda, A. E. Del Rio Castillo, M. Prato, S. Lauciello, F. Bonaccorso, G. Grancini, *J. Mater. Chem. A* **2023**, Advance Article.

[6]   H. Cheng, C. Liu, J. Zhuang, J. Cao, T. Wang, W. Y. Wong, F. Yan, *Adv. Funct. Mater.* **2022**, *32*.

[7]   S. Liu, X. Guan, W. Xiao, R. Chen, J. Zhou, F. Ren, J. Wang, W. Chen, S. Li, L. Qiu, Y. Zhao, Z. Liu, W. Chen, *Adv. Funct. Mater.* **2022**, *32*, 2205009.

[8]   H. Ju, Y. Ma, Y. Cao, Z. Wang, L. Liu, M. Wan, T. Mahmoudi, Y.-B. Hahn, Y. Wang, Y. Mai, *Sol. RRL* **2022**, *6*, 2101082.

[9]   Y.-M. Chang, C.-W. Li, Y.-L. Lu, M.-S. Wu, H. Li, Y.-S. Lin, C.-W. Lu, C.-P. Chen, Y. J. Chang, *ACS Appl. Mater. Interfaces* **2021**, *13*, 6450.

[10] S. Wang, Z. He, J. Yang, T. Li, X. Pu, J. Han, Q. Cao, B. Gao, X. Li, *J. Energy Chem.* **2021**, *60*, 169.

[11] J. Xiong, Z. Dai, S. Zhan, X. Zhang, X. Xue, W. Liu, Z. Zhang, Y. Huang, Q. Dai, J. Zhang, *Nano Energy* **2021**, *84*, 105882.

[12] F. Zhang, Q. Huang, J. Song, S. Hayase, J. Qu, Q. Shen, *Sol. RRL* **2020**, *4*, 2000149.

[13] M. J. Choi, Y. S. Lee, I. H. Cho, S. S. Kim, D. H. Kim, S. N. Kwon, S. I. Na, *Nano Energy* **2020**, *71*, 104639.

[14] W. Chen, F. Z. Liu, X. Y. Feng, A. B. Djurišić, W. K. Chan, Z. B. He, *Adv. Energy Mater.* **2017**, *7*, 1700722.

[15] K. Jiang, J. Wang, F. Wu, Q. Xue, Q. Yao, J. Zhang, Y. Chen, G. Zhang, Z. Zhu, H. Yan, L. Zhu, H. Yip, *Adv. Mater.* **2020**, *32*, 1908011.

[16]   P. Chen, Y. Xiao, L. Li, L. Zhao, M. Yu, S. Li, J. Hu, B. Liu, Y. Yang, D. Luo, C. Hou, X. Guo, J. Shyue, Z. Lu, Q. Gong, H. J. Snaith, R. Zhu, *Adv. Mater.* **2022**, 2206345.

[17]   C. Wang, Z. Su, L. Chen, H. Zhang, W. Hui, D. Liang, G. Zheng, L. Zhang, Z. Tang, W. Wen, J. Tang, Q. Huang, F. Song, Q. Chen, X. Gao, *Appl. Surf. Sci.* **2022**, *571*, 151301.

[18]   Z. Xing, F. Liu, S. Li, Z. Chen, M. An, S. Zheng, A. K. Y. Jen, S. Yang, *Adv. Funct. Mater.* **2021**, *31*, 2107695.

[19]   Q. Cao, J. Yang, T. Wang, Y. Li, X. Pu, J. Zhao, Y. Zhang, H. Zhou, X. Li, X. Li, *Energy Environ. Sci.* **2021**, *14*, 5406.

[20]   S. Wu, Z. Li, J. Zhang, X. Wu, X. Deng, Y. Liu, J. Zhou, C. Zhi, X. Yu, W. C. H. Choy, Z. Zhu, A. K. Y. Jen, *Adv. Mater.* **2021**, *33*, 2105539.

[21]   L. Xu, D. Wu, W. Lv, Y. Xiang, Y. Liu, Y. Tao, J. Yin, M. Qian, P. Li, L. Zhang, S. Chen, O. F. Mohammed, O. M. Bakr, Z. Duan, R. Chen, W. Huang, *Adv. Mater.* **2022**, *34*, 2107111.

[22]   Z. Wang, Y. Lu, Z. Xu, J. Hu, Y. Chen, C. Zhang, Y. Wang, F. Guo, Y. Mai, *Adv. Sci.* **2021**, *8*, 2101856.

[23]   Y. Huang, T. Liu, B. Wang, J. Li, D. Li, G. Wang, Q. Lian, A. Amini, S. Chen, C. Cheng, G. Xing, *Adv. Mater.* **2021**, *33*, 2102816.

[24]   H. Wu, X. Lian, J. Li, Y. Zhang, G. Zhou, X. Wen, Z. Xie, H. Zhu, G. Wu, H. Chen, *J. Mater. Chem. A* **2021**, *9*, 12566.

[25]   X. Lian, J. Chen, S. Shan, G. Wu, H. Chen, *ACS Appl. Mater. Interfaces* **2020**, *12*, 46340.

[26]   Y. Yang, Q. Yuan, H. Li, Y. Niu, D. Han, Q. Yang, Y. Yang, S. Yi, D.-Y. Zhou, L. Feng, *Org. Electron.* **2020**, *86*, 105873.

[27]   H. Liu, H.-R. Liu, F. Yang, J.-E. Yang, J. Song, M. Li, Z. Li, W. C. Tsoi, M. Chinweokwu Eze, Z.-Y. Liu, H. Ma, M. Gao, Z.-K. Wang, *J. Power Sources* **2020**, *448*, 227420.

[28]   H. Wu, X. Lian, S. Tian, Y. Zhang, M. Qin, Y. Zhang, F. Wang, X. Lu, G. Wu, H. Chen, *Sol. RRL* **2020**, *4*, 2000087.

[29]   J. Hu, P. Chen, D. Luo, L. Dai, N. Chen, S. Li, S. Yang, Z. Fu, D. Wang, Q. Gong, S. D. Stranks, R. Zhu, Z. Lu, *Energy Environ. Sci.* **2022**, *15*, 5340.

[30]   X. Hu, C. Liu, Z. Zhang, X. Jiang, J. Garcia, C. Sheehan, L. Shui, S. Priya, G. Zhou, S. Zhang, K. Wang, *Adv. Sci.* **2020**, *7*, 2001285.

[31]   L. Wan, Y. Zhao, Y. Tan, L. Lou, Z.-S. Wang, *Chem. Eng. J.* **2022**, 140569.

[32]   B. Li, J. Deng, J. A. Smith, P. Caprioglio, K. Ji, D. Luo, J. D. McGettrick, K. D. G. I. Jayawardena, R. C. Kilbride, A. Ren, S. Hinder, J. Bi, T. Webb, I. Marko, X. Liu, Y. Xiang, J. Reding, H. Li, S. Du, D. G. Lidzey, S. D. Stranks, T. Watson, S. Sweeney, H. J. Snaith, S. R. P. Silva, W. Zhang, *Adv. Energy Mater.* **2022**, *12*, 2202868.

[33]   J. Yang, T. Wang, Y. Li, X. Pu, H. Chen, Y. Li, B. Yang, Y. Zhang, J. Zhao, Q. Cao, X. Chen, S. Ghasemi, A. Hagfeldt, X. Li, *Sol. RRL* **2022**, *6*, 2200422.